

## **Master's Thesis**

# **Coil-Array Inductive Power Transfer System for Autonomous Underwater Vehicle**

Yu Cheng

Program of Information Science and Engineering  
Graduate School of Information Science  
Nara Institute of Science and Technology

Supervisor: Professor Minoru Okada  
Network Systems Lab. (Division of Information Science)

January 24, 2021

A Master's Thesis  
submitted to Graduate School of Information Science,  
Nara Institute of Science and Technology  
in partial fulfillment of the requirements for the degree of  
MASTER of ENGINEERING

Yu Cheng

Thesis Committee:

Professor Minoru Okada

(Supervisor, Division of Information Science)

Professor Yuichi Hayashi

(Co-supervisor, Division of Information Science)

Associate Professor Takeshi Higashino

(Co-supervisor, Division of Information Science)

Assistant Professor Quang-Thang Duong

(Co-supervisor, Division of Information Science)

Assistant Professor Na Chen

(Co-supervisor, Division of Information Science)

# **Coil-Array Inductive Power Transfer System for Autonomous Underwater Vehicle\***

Yu Cheng

## **Abstract**

For a long time, providing a stable, safe, and efficient power supply for underwater electromechanical equipment has always been a concern in deep-sea exploration. Compared with the complicated docking mechanism, potential safety hazards, and expensive price of traditional wet-mate connectors, wireless power transmission (WPT) technology can transmit energy without any electrical contact between the power supply and the electrical equipment, which provides an effective solution to the aforementioned drawbacks of wired charging. There are many uncontrollable factors in the seawater working environment. Therefore, this topic takes the equivalent circuit and magnetic field distribution as the theoretical basis to study the energy transmission characteristics of underwater WPT and proposes corresponding improvements and solutions to the current problems and deficiencies. Especially for the unstable output voltage of the receiver and excessive magnetic flux density at the internal of AUV. This paper proposes a new type of UWPT system with a coil-array structure, which can reduce the magnetic flux density at the center of the AUV by 40% compared to the conventional hollow cylindrical structure.

## **Keywords:**

Autonomous underwater vehicle, inductive power transfer, underwater wireless power transfer, undersea

---

\*Master's Thesis, Graduate School of Science and Technology, Nara Institute of Science and Technology, January 24, 2021.

# Contents

|   |           |
|---|-----------|
| <b>List of Figures</b>                                    | <b>iv</b> |
| <b>List of Tables</b>                                     | <b>vi</b> |
| <b>1 Introduction</b>                                     | <b>1</b>  |
| 1.1 Background and research purpose . . . . .             | 1         |
| 1.2 Wireless power transfer technologies . . . . .        | 3         |
| 1.3 Underwater wireless power transfer . . . . .          | 5         |
| 1.3.1 Underwater environment . . . . .                    | 5         |
| 1.3.2 Common UWPT systems . . . . .                       | 6         |
| 1.4 The main research content of this thesis . . . . .    | 7         |
| 1.5 Roadmap . . . . .                                     | 7         |
| <b>2 Basic principles of IPT</b>                          | <b>9</b>  |
| 2.1 Inductive coupling model . . . . .                    | 9         |
| 2.2 Compensation network technologies . . . . .           | 10        |
| 2.2.1 S-S compensation topology . . . . .                 | 11        |
| 2.2.2 CLC-S compensation topology . . . . .               | 12        |
| 2.3 Underwater WPT system model . . . . .                 | 13        |
| <b>3 Preliminary exploration of underwater IPT system</b> | <b>16</b> |
| 3.1 The system in three different media . . . . .         | 16        |
| 3.2 The system in different sizes of the coil . . . . .   | 18        |
| 3.3 The system in different frequency . . . . .           | 20        |
| 3.4 Conclusion . . . . .                                  | 20        |
| <b>4 Coil-array WPT</b>                                   | <b>23</b> |
| 4.1 Measurement of the coil-array WPT system . . . . .    | 24        |

|                   |  |           |
|-------------------|--|-----------|
| 4.2               | The other coil arrangements and comparison . . . . .         | 27        |
| 4.3               | Magnetic field distribution . . . . .                        | 28        |
| 4.3.1             | Magnetic field distribution of two-ring strcture . . . . .   | 30        |
| 4.3.2             | Magnetic field distribution of coil-array strcture . . . . . | 32        |
| 4.4               | PET over shift in two directions . . . . .                   | 32        |
| <b>5</b>          | <b>Conclusion</b>  | <b>35</b> |
| 5.1               | Future works . . . . .                                       | 36        |
| <b>References</b> |  | <b>38</b> |

# List of Figures

|     |   |    |
|-----|---|----|
| 1.1 | Underwater sensor networks architecture [12]. . . . .   | 2  |
| 1.2 | Near-field wireless power transfer. . . . .   | 4  |
| 1.3 | Far-field wireless power transfer. . . . .  | 5  |
| 1.4 | Stacked UWPT system [15]. . . . .   | 6  |
| 1.5 | The primary and secondary coils of stacked UWPT system [15]. . . . .  | 6  |
| 1.6 | Plug-in UWPT system [27]. . . . .   | 7  |
| 2.1 | Inductive coupling model. . . . .   | 9  |
| 2.2 | Equivalent circuit of inductive coupling model (T-model). . . . .   | 10 |
| 2.3 | Compensation networks. . . . .  | 11 |
| 2.4 | S-S structure. . . . .  | 12 |
| 2.5 | CLC-S structure. . . . .  | 13 |
| 2.6 | Equivalent circuit of the coil under seawater. . . . .  | 14 |
| 3.1 | Two-ring structure. . . . .   | 16 |
| 3.2 | Two-ring structure ( $r_{inner} = 50mm$ , $r_{outer} = 80mm$ ). . . . .   | 18 |
| 4.1 | Coil-array structure. . . . .   | 23 |
| 4.2 | Sechematic diagram of coil-array UWPT system. . . . .   | 24 |
| 4.3 | Coil-array IPT structure (Both sides with ferrite tile), inner coil in the center or the outer coil. . . . .  | 25 |
| 4.4 | Measurement of $L_s$ . . . . .  | 25 |
| 4.5 | Equivalent circuit of two coil model. . . . .   | 26 |
| 4.6 | Coil-array IPT structure (both sides without ferrite tile), inner coil in the center of the outer coil (left), inner coil next to the outer coil (right). . . . . | 27 |

|      |   |    |
|------|---|----|
| 4.7  | Coil-array IPT structure (both sides without ferrite tile), inner coil<br>in the center of the outer coil (left), inner coil next to the outer<br>coil (right). . . . .   | 28 |
| 4.8  | Coil-array IPT structure (inner small coils with ferrite tile, outer<br>small coils without ferrite tile), inner coil in the center of the outer<br>coil (left), inner coil next to the outer coil (right). . . . . | 29 |
| 4.9  | Two kind of UWPT coil structure simulation diagram. . . . .   | 30 |
| 4.10 | Magnetic field distribution of two-ring IPT structure. . . . .  | 30 |
| 4.11 | Cross-sectional view of the magnetic field distribution of two-ring<br>IPT structure. . . . .   | 31 |
| 4.12 | Magnetic field distribution of coil-array IPT structure. . . . .  | 31 |
| 4.13 | Cross-sectional view of the magnetic field distribution of aoil-array<br>IPT structure. . . . .   | 32 |
| 4.14 | Schematic diagram of direction indication. . . . .  | 33 |
| 4.15 | The PET over shift in two different directions. . . . .   | 34 |

# List of Tables

|     |  |    |
|-----|--|----|
| 1.1 | The different wireless power transmission technologies. . . . .                              | 4  |
| 2.1 | The dielectric constant & conductivity of some materials at 25°C under 1kHz [30,31]. . . . . | 14 |
| 3.1 | The parameters of ring coil structure. . . . .   | 17 |
| 3.2 | The parameters of ring coil structure. . . . .   | 18 |
| 3.3 | Z-parameters in different distance and media . . . . .                                       | 19 |
| 3.4 | The parameters of ring coil structure. . . . .   | 20 |
| 3.5 | Z-parameters in different frequencies and media . . . . .                                    | 21 |
| 4.1 | The parameters of coil-array structure. . . . .  | 24 |
| 4.2 | Maximum power transfer efficiency of different coil arrangements. . . . .                    | 28 |
| 4.3 | The parameters of two coil structure in simulation. . . . .                                  | 29 |

# 1 Introduction

## 1.1 Background and research purpose

In the foreseeable future, electrification of ocean systems, renewable ocean power sources, and ocean energy networks will be necessary because they can help to accelerate the growth of ocean renewable energy and explore the mystery of the ocean [1, 2]. To achieve electrification in the ocean, it is necessary to deploy corresponding sensor networks, which can reliably operate in the underwater environment, to monitor as well as control the electrification system in a timely manner (Figure 1.1). In addition, underwater sensors are also essential equipment for studying the marine environment [3, 4]. They can easily and flexibly explore underwater terrain and ecological environment, which provides convenience for the deployment of underwater sensor networks. Today, one important thing used for exploring the ocean is the autonomous underwater vehicle (UAV). An excellent UAV needs to be equipped with good waterproofness, long-distance controllability, and power durability to operate underwater for a long period of time. For the water-resistance of the equipment, we can use high-performance waterproof and pressure-resistant materials [5–8]. Remote controllability needs to solve the problems of long-distance underwater wireless communication. The durability of electrical equipment requires low energy consumption AUV and high-energy batteries or a continuous power supply. A sufficient power supply can keep underwater sensors and AUVs in an efficient and stable working state for a long time [9]. Indirectly, reducing human interference when electrical equipment is working underwater can also improve work efficiency and reduce deployment costs. Therefore, the power supply for underwater electrical equipment has become a novel research direction. Such methods can solve the energy supply problem of underwater equipment economically and ensure the system perform

long-term and stable work [10, 11].

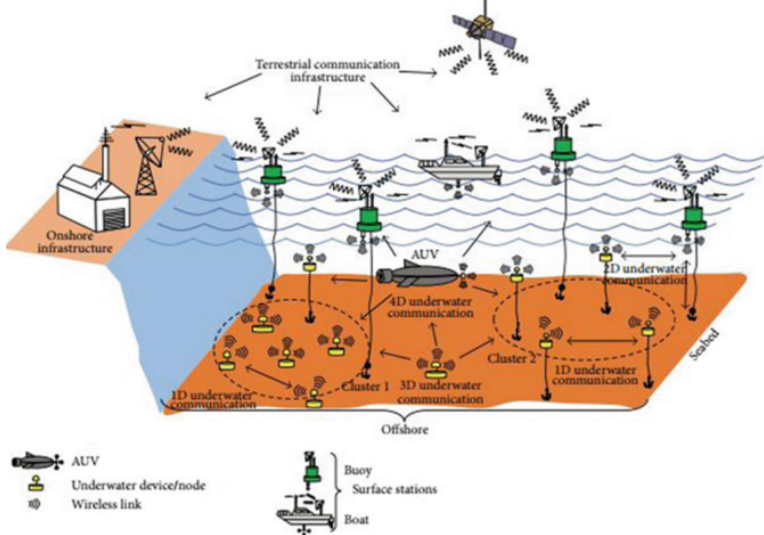


Figure 1.1: Underwater sensor networks architecture [12].

In traditional marine engineering, power is supplied to underwater equipment through wet-mate subsea connectors [13]. For the traditional methods, there have been several challenges, such as wet plug interface technology, its high cost, complex docking method, poor safety performance, and easy to be corroded by seawater [13, 14]. Fortunately, wireless power transfer (WPT) is a potential technology used to deal with these challenges because it can simplify the connection between underwater equipment and power supply, leading to reduce the continuous operating cost of underwater equipment, save a lot of resources. Therefore, more and more scholars have begun to study underwater wireless power transfer (UWPT). [1, 15–18]

There have been many types of energy discovered in the ocean, such as tidal energy, wave energy, marine current power, ocean thermal energy, and sea salinity gradient power [19–22]. Ocean energy is rich, widely distributed, clean, and pollution-free, but low energy density and strong regionality. These advantages make it attractive as grid-connected energy, and may also make it an isolated and remote ocean energy source, thereby providing a valuable source of ocean space. Continuous development provides power solutions that are attractive. The rapid development of distributed ocean energy applications (such as underwater sensor

networks, ocean sensors and monitoring technologies, ocean automatic network buoys, and deep-sea and tsunami buoys) is beneficial. In particular, it can power an AUV whose service life is limited by its battery power.

## 1.2 Wireless power transfer technologies

Broadly speaking, power transfer without direct electrical contact between the primary and secondary is wireless power transfer. WPT technology can be divided into two main categories, near-field (nonradiative region) power transfer and far-field (radiative region) power transfer. Near-field transmission means the distance between primary and secondary sides is within the wavelength ( $\lambda$ ) of the antenna. In turn, the near-field transmission is conventionally divided into two subcategories [23, 24] (Distance between two antennas is denoted by  $D_{range}$ , and diameter of two antenna coils is denoted by  $D_{ant}$ ):

- Short-range when the distance between two antennas is less than the diameter of antenna:  $D_{range} \leq D_{ant}$ . In this range, power is usually transferred through non-resonant capacitive or inductive coupling.
- Mid-range when the distance between two antennas is less than 10 times the diameter of antenna:  $D_{range} \leq 10D_{ant}$ . In this range, energy is usually transferred through resonant capacitive or inductive coupling.

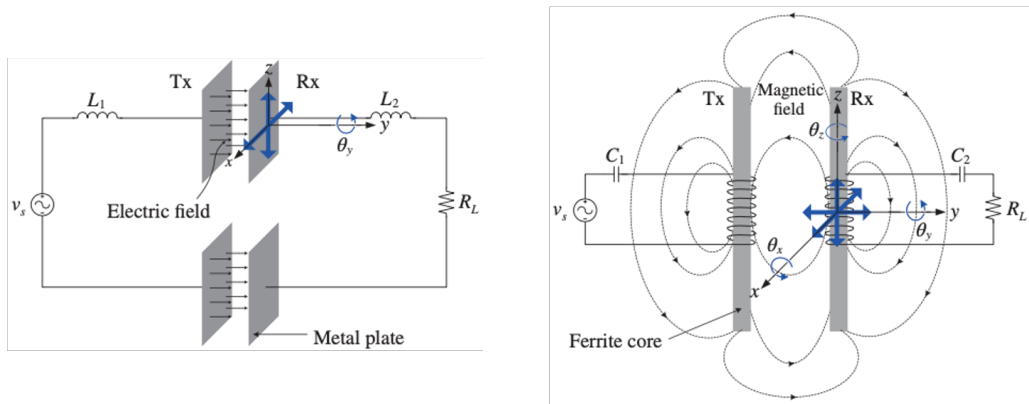
In contrast, in far-field WPT or radiative WPT, power is transmitted by means of electromagnetic waves, like radio waves, microwaves, or light waves. When the operating frequency ( $f$ ) is relatively low, wavelength  $\lambda = c/f$ , at this time the diameter of the antenna is much smaller than the wavelength,  $D_{ant} \ll \lambda$ , and the radiated power will be very small. When the diameter of the antenna is about wavelength,  $D_{ant} \approx \lambda$ , power will be radiated more efficiently. When the diameter of the antenna is much great than the wavelength,  $D_{ant} \gg \lambda$ , we can use high-gain antennas to concentrate electromagnetic waves on a narrow beam and directly aim at the receiver to improve transmission efficiency.

Therefore, near-field wireless power transfer systems mainly include inductive coupling power transfer and capacitive coupling power transfer (Figure 1.2). Far-field wireless power transfer systems mainly include microwave, optical, and

Table 1.1: The different wireless power transmission technologies.

| Technology | Range    | Frequency  | Antenna devices                                   | Applications   |
|------------|----------|------------|---|--|
| Microwaves | hm – km  | GHz        | Parabolic dishes,<br>phased arrays,<br>rectennas  | Satellite, drone<br>aircraft                               |
| Optical    | dam – km | $\geq$ THz | Lasers, photocells,<br>lenses                     | Drone aircraft,<br>space elevator                          |
| Capacitive | cm – m   | kHz – MHz  | Metal plate<br>electrodes                         | Smartcards,<br>biomedical implant                          |
| Inductive  | mm – m   | Hz – GHz   | Tuned wire coils,<br>lumped element<br>resonators | Electric<br>toothbrush,<br>smartphone,<br>electric vehicle |

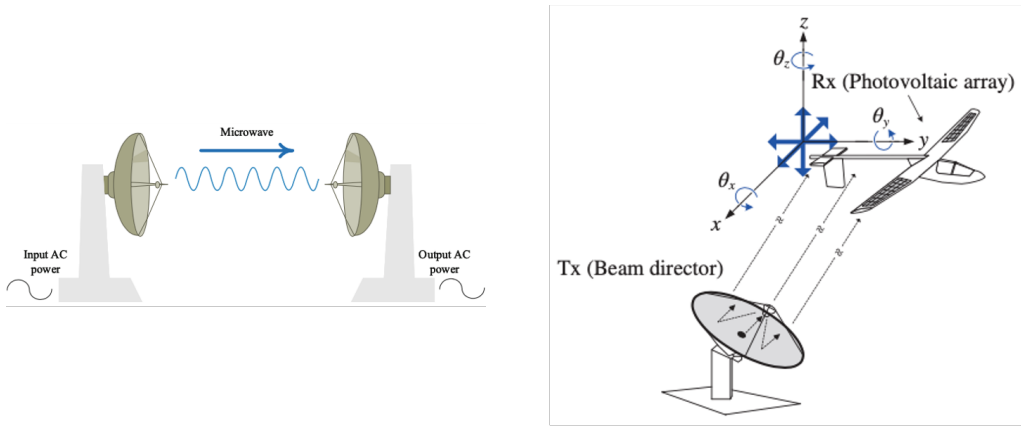
acoustic power transfer (Figure 1.3). The respective characteristics are shown in the table 1.1.



(a) Capacitive power transfer [24].

(b) Inductive power transfer [24].

Figure 1.2: Near-field wireless power transfer.



(a) Microwave power transfer [1].

(b) Laser power transfer [24].

Figure 1.3: Far-field wireless power transfer.

## 1.3 Underwater wireless power transfer

The applications of WPT technology has spread in many fields of science and life. Along with the continuous development of landing application research [25], underwater WPT technology has also attracted the researchers' attention.

### 1.3.1 Underwater environment

Seawater environment has been investigated before [1, 10, 26]. It has several characteristics as follows.

- Underwater and seawater environments have a blocking effect on high-frequency electromagnetic waves. The distance of electromagnetic waves propagating underwater is inversely proportional to the frequency. Therefore, it will be difficult to achieve long-distance power transmission.
- Conductivity should be taken into account in the theoretical analysis due to the electrical conductivity of seawater, which is often omitted in the theoretical analysis of traditional wireless power transmission. Recently, the system model and related theoretical analysis of underwater wireless power transfer technology have been not developed completely.

- The submarine landform is complex and there is the undercurrent. The coupler core is liable to drift underwater. Therefore, the problem of docking between AUV and power stations becomes more challenged when transmission efficiency is sensitive to misalignment between coils.
- Some other impacts consist of microbial enrichment, temperature, salinity.

### 1.3.2 Common UWPT systems

Figure 1.4 shows a stacked UWPT system, this study was completed by Baowei Song et al [15]. They achieved a transmission efficiency of 72% while maintaining 100w output power. They are using a saddle structure transmitter (Details as shown in figure 1.5) and a deformed cylindrical receiver. This structure is very convenient for AUV to park, but because there is no stable protection structure, it is also easy to shift when charging.

Figure 1.6 shows the plug-in UPWT system. It is clear that the AUV needs

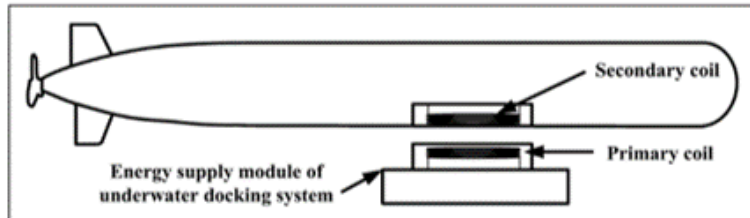


Figure 1.4: Stacked UWPT system [15].

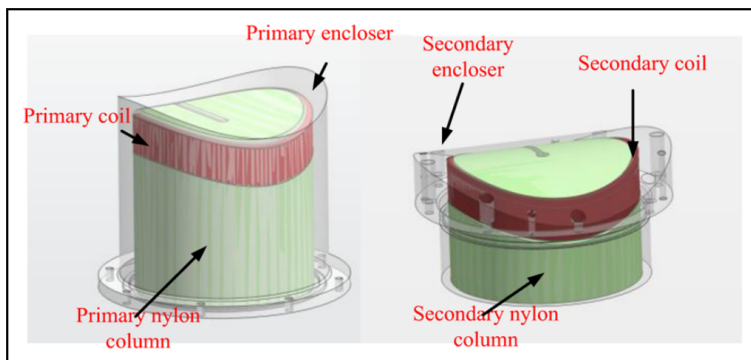


Figure 1.5: The primary and secondary coils of stacked UWPT system [15].

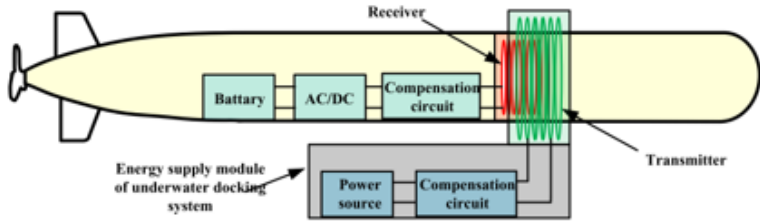


Figure 1.6: Plug-in UWPT system [27].

to be moved into a hollow cylindrical structure transmitter. Conventionally, it will be difficult to park accurately. However, this structure can maintain the stability of the AUV during AUV charging so that the system charging is more secure. Another advantage of this structure is that the receiving coil is relatively large, which can bring out high mutual inductance. As a result, this system can transmit high power to the receiver. However, this structure will generate a higher magnetic field in the middle of the AUV body, which will interfere with or damage the internal electrical components of the AUV. Therefore, in order to address this issue, we propose a coil-array structure UWPT system.

## 1.4 The main research content of this thesis

This thesis mainly investigates the difference between IPT systems in underwater environments and in the air environment. Then, considering the durability and high reliability of underwater AUV, we proposed a novel coil-array power transfer system. By changing the offset of the coil, operating frequency, load resistance, and other variables, we summarized the advantages and disadvantages of the coil-array structure and the traditional hollow cylindrical structure coil. This research can be considered as reference material for subsequent researches on the IPT system using multiple coils in the underwater environment.

## 1.5 Roadmap

The first chapter analyzes the background of this research and its research purpose and significance, analyzes the characteristics and advantages and disadvantages of

mainstream WPT technology, and provides a basis for using IPT technology as an underwater wireless energy transmission system in the following text. A detailed summary and analysis of the current research status of related technologies at home and abroad, including underwater wired energy transmission technology, WPT technology in underwater and air media, and an explanation of the research focus of this article.

The second chapter focuses on the analysis of the basic theory of wireless energy transmission. First, the basic IPT model is explained, and its working principle is analyzed. Then explained the related technology of the compensation network. Finally, analyze the underwater IPT system model.

The third chapter initially explores the influence of the underwater environment on the scene WPT system. First, by measuring the Z-parameter in three different media to observe the changes of the WPT system parameters in different media. Then by changing the size of the internal coil to change the distance between the coils, to judge the change of the WPT system parameters at different distances. Finally, by changing different working frequencies, we can observe the changes of system parameters under different comments.

The fourth chapter first studies the magnetic field characteristics of the different coil structures, focusing on the analysis of the coil size and distance effect on the coil magnetic field, and simulates the magnetic field distribution of the coil in the vacuum, and proposes a new type of coil-array structure. The simulation was carried out by Wipl-d software, and the magnetic field distribution and system transmission efficiency of the coil-array coil structure and the two-ring structure were compared. Then through experiments, we compared the performance of several different coil-array arrangements. Summarize the pros and cons of different arrangements.

Chapter five summarizes the experimental results and some shortcomings in the previous article. In response to these shortcomings, some suggestions that can improve the performance of the experiment are put forward, which are written in future work.

## 2 Basic principles of IPT

This chapter will first introduce the principle of IPT technology from the physical level, and then introduce the principle of IPT technology from the circuit level, analyze the relationship between different equivalent models, and derive system energy transmission indicators that can represent system performance. And analyze the influence of relevant design parameters on system transmission performance. Analyze the influence of the medium on the system performance in the WPT process, and propose an equivalent model in the underwater working environment. Perform simulation analysis on the derivation to ensure that complete theoretical support is provided for more detailed theoretical research and research on new IPT technology.

### 2.1 Inductive coupling model

Figure 2.1 depicts the circuit model of IPT systems, where the transmitting coil  $L_1$  and the receiving coil  $L_2$  are directly connected to the power source and the load, respectively. Denote  $M$  as the mutual inductance,  $r_1$  and  $r_2$  as the equivalent AC resistance of coils.

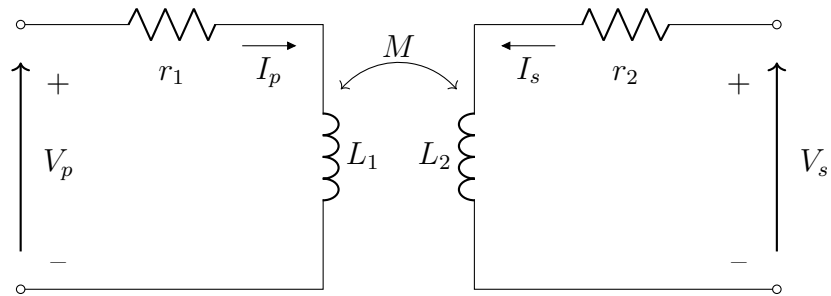


Figure 2.1: Inductive coupling model.

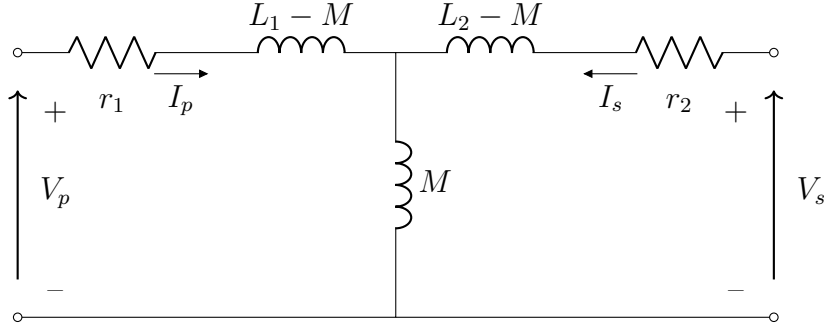


Figure 2.2: Equivalent circuit of inductive coupling model (T-model).

Therefore, the equivalent circuit can be expressed as figure 2.2. According to Kirchhoff's circuit laws. The following formulas can be easily found.

$$V_p = I_p[r_1 + j\omega(L_1 - M)] + (I_p + I_s)j\omega M \quad (2.1)$$

$$= r_1 I_p + j\omega L_1 I_p - j\omega M I_p + j\omega M I_p + j\omega M I_s \quad (2.2)$$

$$= (r_1 + j\omega L_1) I_p + j\omega M I_s \quad (2.3)$$

$$V_s = j\omega M I_p + (r_2 + j\omega L_2) I_s \quad (2.4)$$

The above equations can be expressed as the following matrix equation.

$$\begin{bmatrix} V_p \\ V_s \end{bmatrix} = \begin{bmatrix} r_1 + j\omega L_1 & j\omega M \\ j\omega M & r_2 + j\omega L_2 \end{bmatrix} \begin{bmatrix} I_p \\ I_s \end{bmatrix} \quad (2.5)$$

If we use  $\mathbf{V}$ ,  $\mathbf{Z}$ ,  $\mathbf{I}$  to express the corresponding matrices. The formula 2.5 can be represented as follows.

$$\mathbf{V} = \mathbf{Z} \cdot \mathbf{I} \quad (2.6)$$

Here, the imaginary part of  $Z_{11}$  ( $j\omega L_1$ ) and  $Z_{22}$  ( $j\omega L_2$ ) can be canceled by the compensation networks.

## 2.2 Compensation network technologies

A compensation network is a network that makes some adjustments to compensate for system electrical defects. If capacitor compensation is used only on the

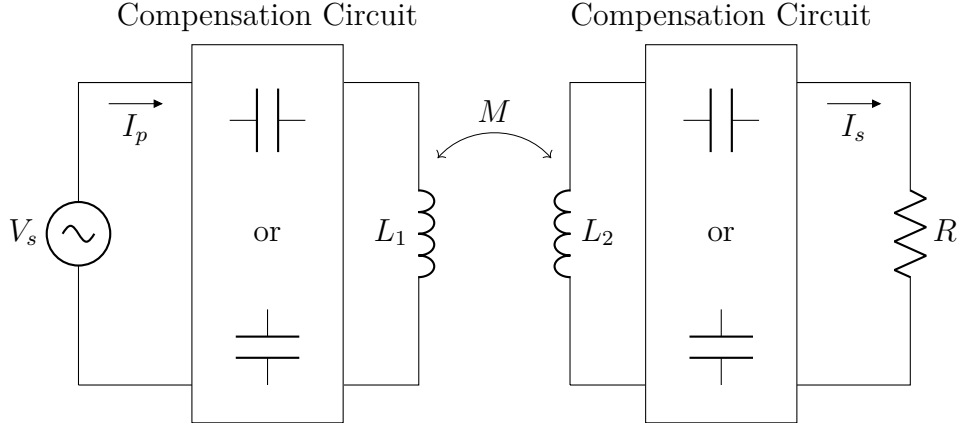


Figure 2.3: Compensation networks.

primary or secondary side, it is called single-sided compensation topology; when capacitor compensation is used on both the primary and secondary sides at the same time, it is called double-sided compensation topology. The calculation of the capacitance value of single-sided compensation is relatively simple, but the actual effect is not as good as the double-sided compensation method. Therefore, this article only discusses bilateral compensation. As shown in the figure 2.3, according to the different connection modes of the capacitors on both sides, common resonance compensation technologies can be divided into four structures: S-S, S-P, P-S, P-P (S denotes series and P denotes parallel). In addition, there are more complicated compensation networks such as CLC and LCC [28, 29].

Since only S-S topology and CLC-S topology are used in the following contents, we only analyze these two compensation topologies in detail here.

### 2.2.1 S-S compensation topology

When the inductors and the capacitors in the resonance state, we have,

$$\omega = \omega_0 = \frac{1}{\sqrt{LC}}, \quad (2.7)$$

where  $\omega$  represents the working frequency,  $\omega_0$  represents the resonant angular frequency of the circuit. Here, to maximize the transmission efficiency of the WPT system, we need to make the resonant frequencies of the primary side and

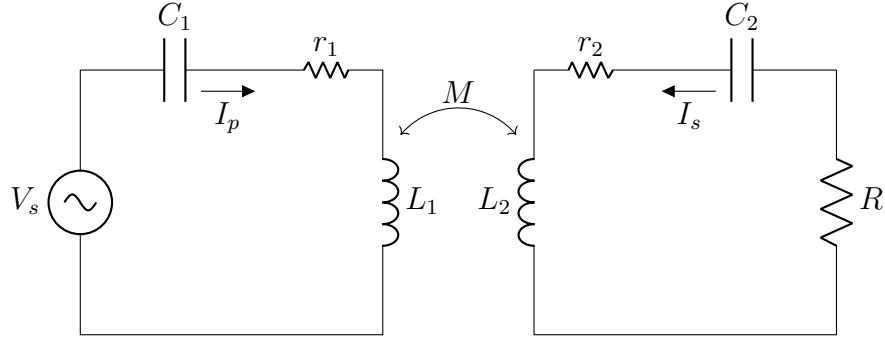


Figure 2.4: S-S structure.

secondary side consistent. Therefore,

$$\omega_0 = \frac{1}{L_1 C_1} = \frac{1}{L_2 C_2} \quad (2.8)$$

For any formed coil, we can measure its corresponding inductance value at a specified frequency. Thus, we can get the value of the compensation capacitor by formula 2.9.

$$C = \frac{1}{\omega_0^2 L} \quad (2.9)$$

The compensation network of S-S structure is shown in figure 2.4. The relationship between load voltage  $V_R$  and power source voltage  $V_s$  of SS topology shows below,

$$V_R = \frac{j\omega MR}{(R + r_1)r_0 + \omega^2 M^2} V_s. \quad (2.10)$$

### 2.2.2 CLC-S compensation topology

The compensation network of CLC-S structure is shown as in figure 2.5. According to the Kirchhoff's circuit laws we can get the following equations.

$$V_s = -jX_C I_s + jX_L I_L \quad (2.11)$$

$$V_0 = (-jX_{C_0} + jX_{L_0} + r_0)I_0 + j\omega M I_1 \quad (2.12)$$

$$V_R = j\omega I_0 + (-jX_{C_1} + jX_{L_1} + r_1)I_1 \quad (2.13)$$

$$V_R = -RI_1 \quad (2.14)$$

$$I_s = I_L + I_0 \quad (2.15)$$



Figure 2.5: CLC-S structure.

Therefore, the relationship between load voltage  $V_R$  and power source voltage  $V_s$  of CLC topology can be expressed as below,

$$V_R = -\frac{R}{R+r_1} \cdot \frac{\omega M}{X_L} V_s. \quad (2.16)$$

Because  $r_1$  is the internal resistance of the  $L_1$  coil, its value is very small, and  $\frac{\omega M}{X_L}$  is a constant value at a certain operating frequency. We can see that when  $R \gg r_1$ ,  $\frac{R}{R+r_1} \approx 1$ , which means the voltage of load  $V_R$  will not be affected by load resistance  $R$ .

## 2.3 Underwater WPT system model

In the seawater environment, the electrical parameters of seawater as the transmission medium are quite different from those in the air, as shown in the table 2.1.

It can be seen from table 2.1 that the relative permittivity of seawater is larger than that of air medium, resulting in a distributed capacitance between two conductors that are relatively close in seawater; at the same time, seawater has a certain conductivity , This is equivalent to connecting an eddy current loss resistor in series at both ends of the coil. Eddy current loss resistance and distributed capacitance will affect the impedance of the coil and generate additional power loss. Therefore, the conventional mutual inductance model of formula 2.5. cannot

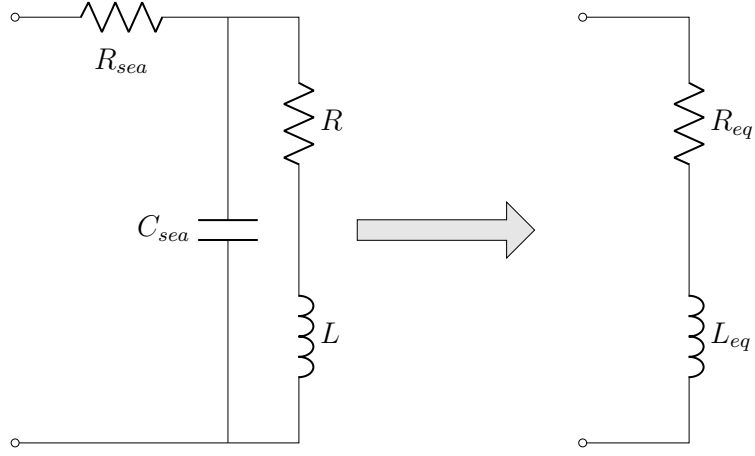


Figure 2.6: Equivalent circuit of the coil under seawater.

reflect the influence of seawater media on transmission, and cannot completely and accurately describe the transmission behavior under seawater.

As shown in figure 2.6,  $R_{sea}$  is the eddy current loss resistance,  $C_{sea}$  is the distributed capacitance, both of which increase with the increase of operating frequency,  $R$  is the internal resistance of the coil itself, and  $L$  is the coil inductance. The mathematical expressions of equivalent inductance  $L_{eq}$  and equivalent resistance  $R_{eq}$  are as follows,

$$L_{eq} = \frac{L - \omega^2 L^2 C_{sea} - C_{sea} R^2}{(1 - \omega^2 L C_{sea})^2 + \omega^2 C_{sea}^2 R^2}, \quad (2.17)$$

Table 2.1: The dielectric constant & conductivity of some materials at 25°C under 1kHz [30, 31].

| Material         | Relative permittivity | Conductivity             |
|------------------|-----------------------|--------------------------|
| Vacuum           | 1                     | 0 S/m                    |
| Air              | 1.0006                | 0 S/m                    |
| Ultra pure water | 81                    | $5.5 \times 10^{-6}$ S/m |
| Drinking water   | 81                    | 0.005 – 0.05 S/m         |
| Seawater         | 81                    | 5 S/m                    |

and

$$R_{eq} = R_{sea} + \frac{R}{(1 - \omega^2 LC_{sea})^2 + \omega^2 C_{sea}^2 R^2}. \quad (2.18)$$

Where  $\omega$  is the operating angular frequency. Generally speaking, eddy current loss resistance  $R_{sea}$  and distributed capacitance  $C_{sea}$  are affected by many factors and are difficult to measure. Therefore, equations 2.17 and 2.18 are not easy to calculate, and they are usually obtained with three-dimensional electromagnetic field simulation software or experiments. Since  $R_{eq}$  is generally larger at high frequencies, underwater magnetic coupling resonance wireless energy transmission generally uses a working frequency below 1 MHz.

### 3 Preliminary exploration of underwater IPT system

In order to explore the similarities and differences between the wireless energy transmission system in the seawater environment and the wireless energy transmission system in the air in the actual situation, a simple double-coil structure is used to explore the electrical properties of the underwater environment. This chapter will introduce the performance of the double coil structure working in sea water.

#### 3.1 The system in three different media

In order to design a wireless power transmission system suitable for underwater AUV, we will first use hollow cylindrical structure transmitter and cylindrical



(a) Experimental coil.



(b) Structure diagram.

Figure 3.1: Two-ring structure.

Table 3.1: The parameters of ring coil structure.

| Items                             | Parameters               |
|-----------------------------------|--------------------------|
| Environment                       | Air, tap water, seawater |
| Wire diameter                     | 0.8mm                    |
| Wire material                     | Copper                   |
| Tx coil diameter                  | 113mm                    |
| Rx coil diameter                  | 85mm                     |
| Turns (Inner coil and outer coil) | 10                       |
| Frequency                         | 200kHz                   |

structure receiver to explore the performance of the UWPT system of this plug-in structure UWPT in water. For the convenience of writing, it will be referred to as a double ring structure in the following text. The coil structure as shown in figure 3.1.

Its detailed parameters are shown in Table 3.1.

When we use the vector network analyzer (VNA) to place the coil in the air, tap water, or sea water for measurement, the following data can be obtained:

$$Z_{air} = \begin{bmatrix} 0.4 + 29.6i & 0.0 - 10.0i \\ 0.0 - 10.0i & 0.3 + 20.3i \end{bmatrix},$$

$$Z_{tap-water} = \begin{bmatrix} 3.0 + 32.1i & -1.5 - 11.3i \\ -1.5 - 11.3i & 1.5 + 21.6i \end{bmatrix},$$

$$Z_{seawater} = \begin{bmatrix} 7.2 + 37.8i & -6.0 - 15.7i \\ -6.0 - 15.7i & 6.5 + 25.3i \end{bmatrix}.$$

In the above measurement results, we can find that as the transmission medium changes (from air to tap-water to seawater), each corresponding value is increasing. It illustrates that the internal resistances of the coils are small in the air. However, the internal resistances significantly increase when the coils are in tap-water or seawater. This may deteriorate the transmission efficiency as well as the load voltage stability. In addition, the mutual inductance between two coils becomes complex number and the self-inductances of the coils slightly increase.

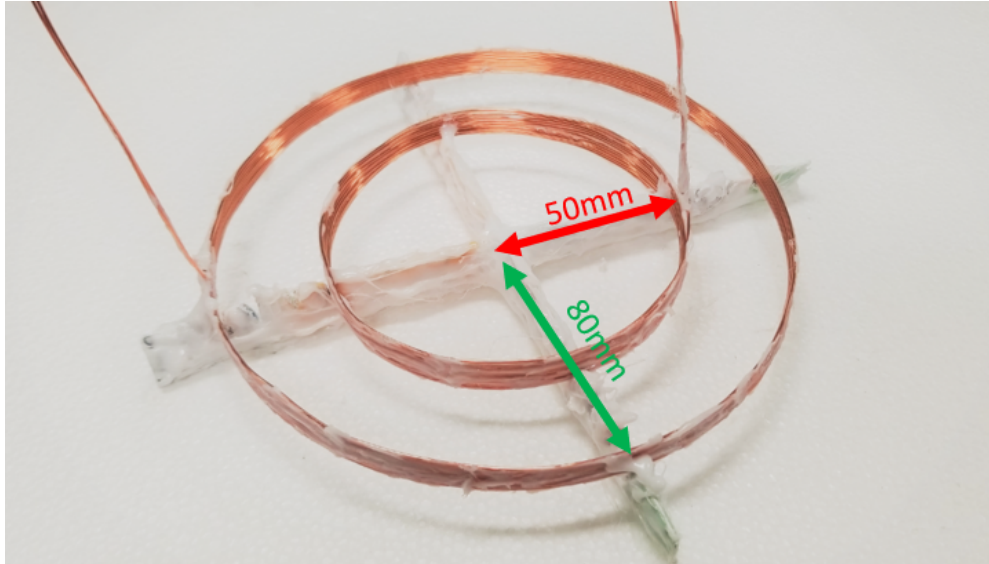


Figure 3.2: Two-ring structure ( $r_{inner} = 50\text{mm}$ ,  $r_{outer} = 80\text{mm}$ ).

### 3.2 The system in different sizes of the coil

In order to explore the influence of the size of the internal coil and the distance between the two coils on the system (Figure 3.2), the coil size is changed here to change the distance between the transmitter and the receiver. The specific parameters are as follows (Table 3.2).

After changing the medium between the coils and the distance between the coils, the Z-parameters in different scenarios are measured by VNA, and we get

Table 3.2: The parameters of ring coil structure.

| Items                             | Parameters               |
|-----------------------------------|--------------------------|
| Environment                       | Air, tap water, seawater |
| Wire diameter                     | 0.8mm                    |
| Wire material                     | Copper                   |
| Tx coil diameter                  | 160mm                    |
| Rx coil diameter                  | 100mm, 120mm, 140mm      |
| Turns (Inner coil and outer coil) | 10                       |
| Frequency                         | 200kHz                   |

Table 3.3: Z-parameters in different distance and media

| Media     | Coil size<br>(Radius) | Distance | Z-parameter  |
|-----------|-----------------------|----------|--|
| Air       | 80mm - 50mm           | 30mm     | $\begin{bmatrix} 0.6826 + 46.4075i & -0.0411 - 8.9620i \\ -0.0382 - 8.9669i & 0.3423 + 24.2260i \end{bmatrix}$   |
|           | 80mm - 60mm           | 20mm     | $\begin{bmatrix} 0.7194 + 46.1416i & -0.0946 - 15.0048i \\ -0.0906 - 15.0155i & 0.5225 + 32.5246i \end{bmatrix}$ |
|           | 80mm - 70mm           | 10mm     | $\begin{bmatrix} 0.6657 + 45.9561i & 0.0757 + 24.2562i \\ 0.0699 + 24.2747i & 0.5651 + 39.2948i \end{bmatrix}$   |
| Tap-water | 80mm - 50mm           | 30mm     | $\begin{bmatrix} 5.4603 + 53.0814i & -2.4332 - 11.7753i \\ -2.4304 - 11.7859i & 1.7722 + 26.0449i \end{bmatrix}$ |
|           | 80mm - 60mm           | 20mm     | $\begin{bmatrix} 7.0513 + 54.2993i & -4.4889 - 20.1926i \\ -4.4867 - 20.2100i & 3.9114 + 36.7652i \end{bmatrix}$ |
|           | 80mm - 70mm           | 10mm     | $\begin{bmatrix} 2.8768 + 49.8765i & 0.9991 + 26.5644i \\ 0.9946 + 26.5864i & 1.9865 + 42.0751i \end{bmatrix}$   |
| Seawater  | 80mm - 50mm           | 30mm     | $\begin{bmatrix} 1.761 + 58.2022i & -0.554 - 14.5303i \\ -0.5512 - 14.5424i & 0.6543 + 27.6708i \end{bmatrix}$   |
|           | 80mm - 60mm           | 20mm     | $\begin{bmatrix} 2.0488 + 61.1579i & -0.9906 - 25.1528i \\ -0.9814 - 25.1736i & 1.2212 + 40.4982i \end{bmatrix}$ |
|           | 80mm - 70mm           | 10mm     | $\begin{bmatrix} 2.0347 + 52.4298i & 0.4957 + 27.1092i \\ 0.4843 + 27.1321i & 1.4439 + 43.4828i \end{bmatrix}$   |

the following results (Table 3.3).

In table 3.3, we can find that under the same medium, as the internal coil decreases, the transmission distance increases. We can see that the imaginary part of  $Z_{11}$  and  $Z_{22}$  are increasing, indicating that the impedance of the coil is increasing.

Table 3.3 shows the measures of Z-parameter of the coupling network under

Table 3.4: The parameters of ring coil structure.

| Items                             | Parameters                             |
|-----------------------------------|--|
| Environment                       | Air, seawater                          |
| Wire diameter                     | 0.8mm                                  |
| Wire material                     | Copper                                 |
| Tx coil diameter                  | 160mm                                  |
| Rx coil diameter                  | 100mm                                  |
| Turns (Inner coil and outer coil) | 10                                     |
| Frequency                         | 100kHz, 150kHz, 200kHz, 250kHz, 300kHz |

several cases of coil sizes and distances in air, tap-water and seawater. In general, self-inductance of coil increases as coil size increases. The mutual inductance between two coils increases as the distance between them decreases. The internal resistances of the coils are small in air and larger in tapwater as well as seawater.

### 3.3 The system in different frequency

Earlier we have studied the z-parameter changes of the two-ring coil structure under different media and different distances. In this section we will study how z-parameters changes at different frequencies. Table 3.4 a shows the parameters of the experiment.

After using the above parameters, we got the following results (Table 3.5).

Table 3.5 shows that the internal resistances of the coils are less than  $1\Omega$  in the air when operating frequency changes from 100kHz to 300kHz. However, under seawater environment, the internal resistances of the coils are smaller than  $1\Omega$  when the operating frequency is under 200kHz. As the operating frequency is over 200kHz, the internal resistances of the coils significantly increase.

### 3.4 Conclusion

This section illustrated the measures of the coupling network in air, under tap-water and under seawater with different operating frequencies. The measures in-

Table 3.5: Z-parameters in different frequencies and media

| Media    | Frequency | Z-parameter  |
|----------|-----------|--|
| Air      | 100kHz    | $\begin{bmatrix} 0.3758 + 23.2130i & -0.0036 - 4.4495i \\ -0.0012 - 4.4520i & 0.2123 + 12.1526i \end{bmatrix}$           |
|          | 150kHz    | $\begin{bmatrix} 0.4789 + 34.7320i & -0.0074 - 6.6739i \\ -0.0037 - 6.6774i & 0.2575 + 18.1971i \end{bmatrix}$           |
|          | 200kHz    | $\begin{bmatrix} 0.5755 + 46.2288i & -0.0121 - 8.9004i \\ -0.0050 - 8.9065i & 0.3031 + 24.2211i \end{bmatrix}$           |
|          | 250kHz    | $\begin{bmatrix} 0.6737 + 57.7432i & -0.0153 - 11.1342i \\ -0.0095 - 11.1426i & 0.3423 + 30.2465i \end{bmatrix}$         |
|          | 300kHz    | $\begin{bmatrix} 0.7556 + 69.2691i & -0.0191 - 13.3746i \\ -0.0100 - 13.3859i & 0.3791 + 36.2676i \end{bmatrix}$         |
| Seawater | 100kHz    | $\begin{bmatrix} 0.5314 + 24.3255i & -0.0760 - 4.9832i \\ -0.0717 - 4.9862i & 0.2593 + 12.5247i \end{bmatrix}$           |
|          | 150kHz    | $\begin{bmatrix} 0.9900 + 39.2700i & -0.2453 - 8.8345i \\ -0.2392 - 8.8400i & 0.4080 + 19.6434i \end{bmatrix}$           |
|          | 200kHz    | $\begin{bmatrix} 2.0236 + 59.0193i & -0.7053 - 15.0451i \\ -0.6942 - 15.0581i & 0.7248 + 28.1895i \end{bmatrix}$         |
|          | 250kHz    | $\begin{bmatrix} 4.8486 + 89.4034i & -2.0763 - 26.6084i \\ -2.0597 - 26.6276i & 1.5345 + 39.8440i \end{bmatrix}$         |
|          | 300kHz    | $10^2 \times \begin{bmatrix} 0.1548 + 1.4909i & -0.0751 - 0.5327i \\ -0.0749 - 0.5333i & 0.0450 + 0.5985i \end{bmatrix}$ |

dicated that the internal resistances of the coils would increase when the system operated under tapwater or seawater. This would reduce transmission efficiency.

Moreoever, it could also make load voltage unstable against load variations even though CLC topology was employed. The internal resistances increased significantly as the operating frequency increased over 200kHz. Therefore, the system should operate at the frequency of lower than 200kHz under tapwater or seawater environment to restrict the loss caused by internal resistances.

## 4 Coil-array WPT

Through the explanation in the previous chapter, we know the basic performance of the wireless transmission system underwater. This chapter will introduce the underwater coil-array WPT system we designed, by degrading a large double coil structure into multiple mini-coils structures, as shown in figure 4.1. This greatly reduces the magnetic field in the internal coil, thereby achieving electromagnetic protection inside the AUV system. Its detailed parameters are shown in table 4.1.

In the marine environment, we can use buoys to generate electricity [1], store the collected electricity in the power source, and then connect the power source to the transmitter (Tx). When the AUV (Rx) reaches the designated position of the transmitter, the AUV can be charged wirelessly. This is the basic workflow of this UWPT system. Figure 4.2 shows a schematic diagram of the UWPT system.

In the following subsections, the performance of the coil-array UWPT system

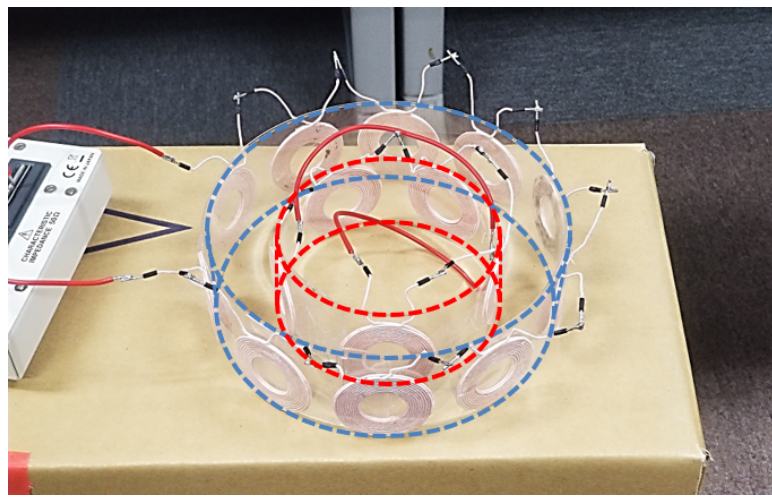


Figure 4.1: Coil-array structure.

Table 4.1: The parameters of coil-array structure.

| Items                  | Parameters               |
|------------------------|--------------------------|
| Tx coil diameter       | 160mm                    |
| Rx coil diameter       | 100mm                    |
| The number of Tx coils | 10                       |
| The number of Rx coils | 5                        |
| Mini-coil connection   | In series                |
| Mini-coil model        | WE 760308110 (Litz wire) |

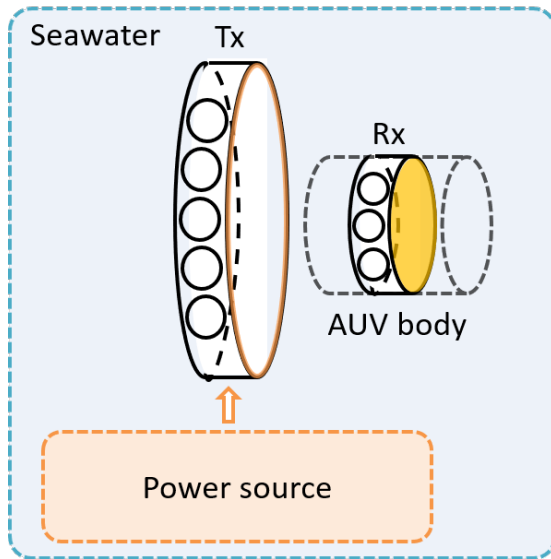


Figure 4.2: Sechematic diagram of coil-array UWPT system.

will be described in detail.

## 4.1 Measurement of the coil-array WPT system

In this section, we will first introduce different coil arrangements. By changing the coil structure of the coil-array, observe the performance of the changed coil structure under different conditions.

As shown in figure 4.3, a transmitter coil with a radius of 80mm is used here, which consists of 10 coils with ferrite in series, and a receiver coil with a radius



| Parameters             |   | Inner coil (Tx) | Outer coil (Rx) |
|------------------------|---|-----------------|-----------------|
| Diameter               |   | 100mm           | 160mm           |
| Number of coils        |   | 5               | 10              |
| Material               |   | Litz wire (2mm) | Litz wire (2mm) |
| 200kHz                 | Q | 207             | 206.25          |
|                        | L | $125.01\mu H$   | $241.03\mu H$   |
| Position of inner coil |   | center          |                 |
| $L_s$                  |   | $240.65\mu H$   |                 |
| $M$                    |   | 6.8923          |                 |
| $k$                    |   | 0.0397          |                 |
| $kQ$                   |   | 8.2007          |                 |
| $\eta_{max}$           |   | 78.41%          |                 |

Figure 4.3: Coil-array IPT structure (Both sides with ferrite tile), inner coil in the center or the outer coil.

of 50mm, which consists of 5 coils with ferrite in series. Therefore, the distance between Tx and Rx is 30mm. For other specific parameters, please find in the figure 4.3.

By using LCR meter to measure this arrangement system, we can get the inductance of the Tx's coil-array coil,  $L_1 = 241.03\mu H$ , and quality factor  $Q_1 = 206.25$ . And the inductance of Rx's coil-array coil,  $L_2 = 125.01\mu H$ , and quality factor  $Q_2 = 207$ . Then short-circuit the Rx coil and place it in the middle of the Tx coil, and measure the inductance of the Tx in this state (As shown in figure 4.4), which is  $L_s$ , where  $L_s = 240.65\mu H$ .

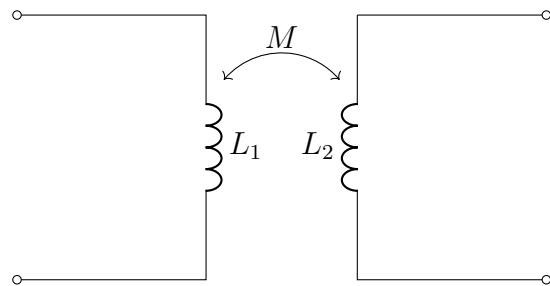


Figure 4.4: Measurement of  $L_s$ .

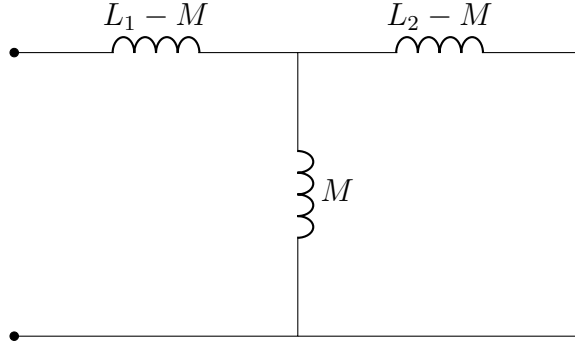


Figure 4.5: Equivalent circuit of two coil model.

From equivalent circuit (Figure 4.5), we can get the following formula.

$$L_s = L_1 - M + \frac{M(L_2 - M)}{L_2}. \quad (4.1)$$

Move  $M$  to the left side of the equation, the mutual inductance can be expressed as,

$$M = \sqrt{L_2(L_1 - L_s)}, \quad (4.2)$$

and coupling coefficient,

$$k = \frac{M}{L_1 L_2}. \quad (4.3)$$

$kQ$  product can be expressed as,

$$kQ = k\sqrt{Q_1 Q_2}. \quad (4.4)$$

$kQ$  product is an index showing the performance of a wireless transfer. The relationship between the maximum transmission efficiency  $\eta_{max}$  and  $kQ$  as follows [32, 33],

$$\eta_{max} = \frac{k^2 Q_1 Q_2}{(1 + \sqrt{1 + k^2 Q_1 Q_2})^2}. \quad (4.5)$$

According to the calculation of the above formula, we can get that the maximum transmission efficiency  $\eta_{max}$  of this arrangement is 78.41%.

## 4.2 The other coil arrangements and comparison

Next, we will observe the performance of the system under different conditions by increasing the number of coils and changing the position of the Rx coil in the Tx coil. The result is shown in the figure 4.6, figure 4.7, and figure 4.8.

Through the results under each of the above scenarios, we can summarize them into table 4.2, as follows

From table 4.2, we can get the following conclusions:

- When we increase the number of inner coils from 5 to 6, the maximum PTE (Power transfer efficiency) will increase.
- If the numbers of outer and inner coils are the same, when outer coils without ferrite and inner coils with ferrite, we can get the maximum PTE.
- When there is no ferrite outside the inner coil, the PTE will increase if the inner coil deviates from the middle, and vice versa.

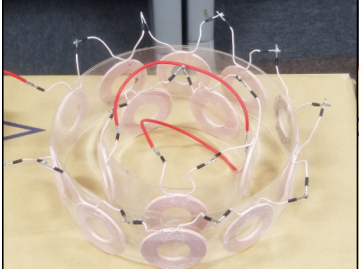
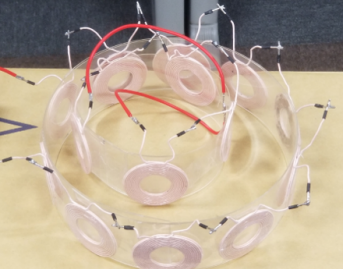
| Number of outer coils   |  | Number of inner coils |         |
|---|--|-----------------------|---------|
| 10  | 5  |                       |         |
|  |  |                       |         |
| $M$   | 4.2371   | $M$                   | 8.9941  |
| $k$   | 0.0428   | $k$                   | 0.0909  |
| $kQ$  | 7.5365   | $kQ$                  | 15.9979 |
| $\eta_{max}$  | 76.75%   | $\eta_{max}$          | 88.26%  |

Figure 4.6: Coil-array IPT structure (both sides without ferrite tile), inner coil in the center of the outer coil (left), inner coil next to the outer coil (right).

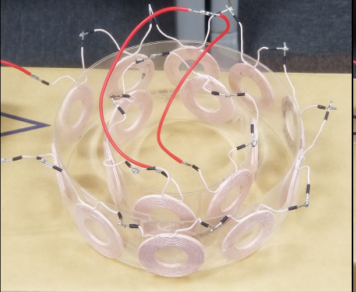
| Number of outer coils   |  | Number of inner coils |         |
|---|--|-----------------------|---------|
| 10  | 6  |                       |         |
|  |  |                       |         |
| $M$   | 4.7709   | $M$                   | 13.4385 |
| $k$   | 0.0446   | $k$                   | 0.1255  |
| $kQ$  | 7.6436   | $kQ$                  | 21.5303 |
| $\eta_{max}$  | 77.03%   | $\eta_{max}$          | 91.13%  |

Figure 4.7: Coil-array IPT structure (both sides without ferrite tile), inner coil in the center of the outer coil (left), inner coil next to the outer coil (right).

Table 4.2: Maximum power transfer efficiency of different coil arrangements.

| Shift                            | Numbers of coil (Outer - Inner) | Both coils with ferrite | Both coils without ferrite | Outer coils without ferrite, inner coils with ferrite |
|----------------------------------|---------------------------------|-------------------------|----------------------------|---|
| Inner coil in the center         | 10 - 5                          | 78.41%                  | 76.75%                     | 84.95%  |
|                                  | 10 - 6                          |                         | 77.03%                     |   |
| Inner coil close to the one side | 10 - 5                          |                         | 88.26%                     | 78.80%  |
|                                  | 10 - 6                          |                         | 91.13%                     |   |

### 4.3 Magnetic field distribution

In order to clarify the magnetic field distribution of the coil-array structure, we used Wipl-d electromagnetic simulation software. We simulated the following two

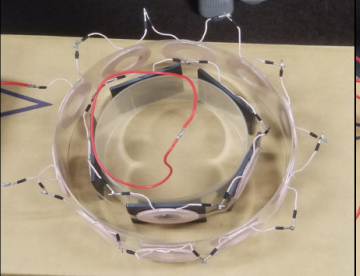
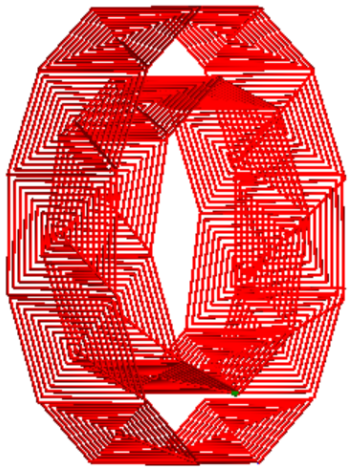
| Number of outer coils   |  | Number of inner coils |        |
|---|--|-----------------------|--------|
| 10  | 5  |                       |        |
|  |  |                       |        |
| $M$   | 8.3363   | $M$                   | 5.8093 |
| $k$   | 0.0629   | $k$                   | 0.0435 |
| $kQ$  | 12.2445  | $kQ$                  | 8.3768 |
| $\eta_{max}$  | 84.95%   | $\eta_{max}$          | 78.81% |

Figure 4.8: Coil-array IPT structure (inner small coils with ferrite tile, outer small coils without ferrite tile), inner coil in the center of the outer coil (left), inner coil next to the outer coil (right).

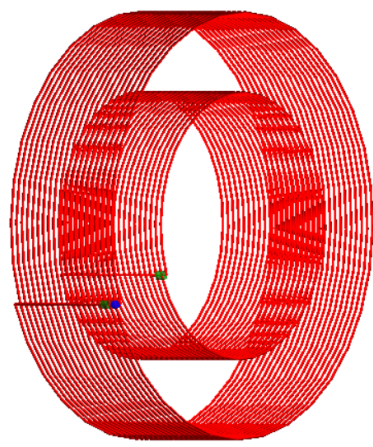
Table 4.3: The parameters of two coil structure in simulation.

| Items                  | Coil-array structure | Two-ring structure |
|------------------------|----------------------|--------------------|
| Tx coil diameter       | 160mm                | 160mm              |
| Rx coil diameter       | 100mm                | 100mm              |
| The number of Tx coils | 12                   | 1                  |
| The number of Rx coils | 8                    | 1                  |
| Wire material          | Copper               | Copper             |
| Frequency              | 200kHz               | 200kHz             |
| Resistance of load     | $5\Omega$            | $5\Omega$          |
| Voltage of source      | 6v                   | 64v                |
| Output power           | 10w                  | 10w                |

structures as shown in figure 4.9, and the specific parameters are as table 4.3.



(a) Coil-array IPT structure.



(b) Two-ring IPT structure.

Figure 4.9: Two kind of UWPT coil structure simulation diagram.

#### 4.3.1 Megnetic field distribution of two-ring strcture

In order to judge whether the coil-array structure can reduce the internal magnetic field strength of the AUV system, we first simulated the conventional two-ring structure. The results are shown in figure 4.10 and figure 4.11. figure 4.10 shows the magnetic field distribution between the transmitting and receiving coils in a three-dimensional space. The highest peak in the figure is the middle of the two

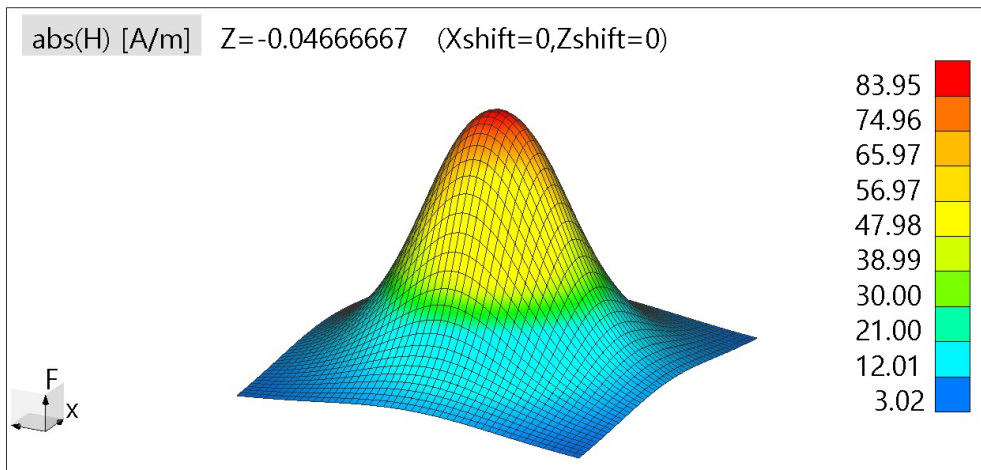


Figure 4.10: Magnetic field distribution of two-ring IPT structure.

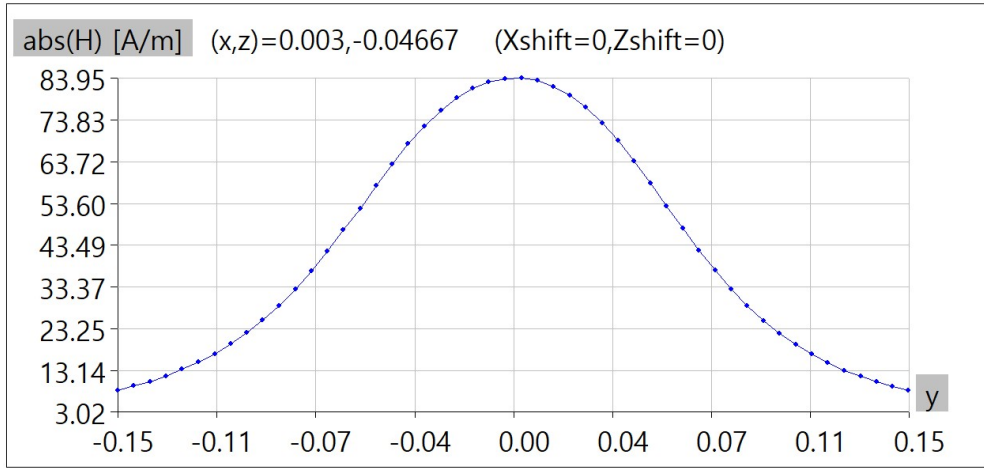


Figure 4.11: Cross-sectional view of the magnetic field distribution of two-ring IPT structure.

coils, that is, the magnetic field distribution shown in figure 4.10 is generated inside the AUV. figure 4.11 is a cross-sectional view of figure 4.10 from the side. We can see that the magnetic induction intensity of the middle part has reached  $83.95A/m$ , and the other parts are gradually decreasing, like a mountain.

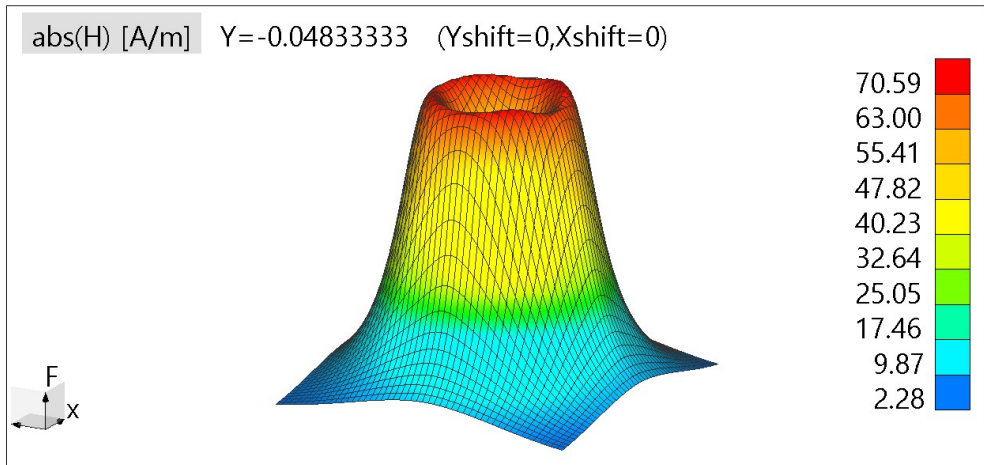


Figure 4.12: Magnetic field distribution of coil-array IPT structure.

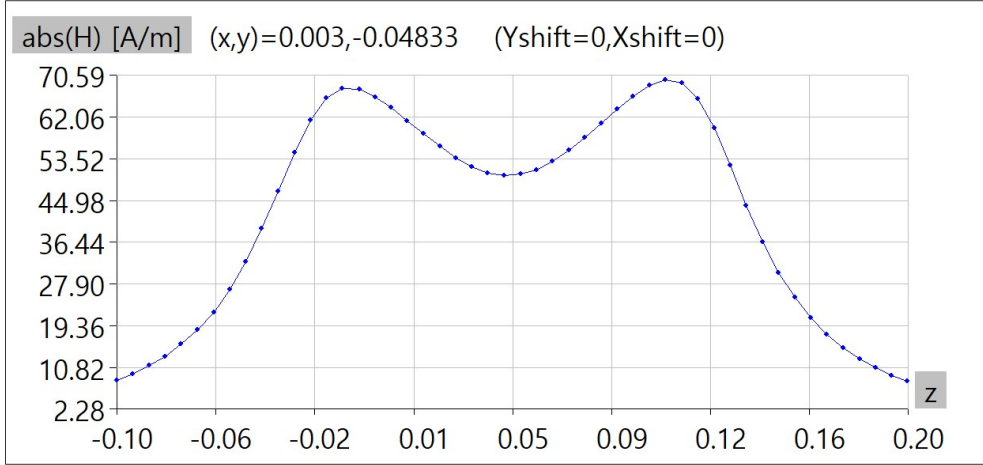


Figure 4.13: Cross-sectional view of the magnetic field distribution of a coil-array IPT structure.

### 4.3.2 Magnetic field distribution of coil-array structure

After completing the simulation of the magnetic field distribution of the two-ring structure, we did the same simulation on the coil-array structure coil, and the results are shown in figure 4.12 and figure 4.13. In figure 4.12, we can see that the magnetic field distribution of the coil-array structure is like a volcano, with low magnetic induction in the middle part and high surrounding magnetic induction. The part with the highest magnetic induction is between the two coils, that is, outside the AUV, which will not affect the inside of the AUV system. From figure 4.13 we can see that the internal magnetic field of the AUV is around 50A/m, which is 40% lower than the two-ring structure, and its large magnetic induction intensity is lower than 70A/m, which is lower than the highest magnetic induction intensity of the two-ring structure 13A/m.

## 4.4 PET over shift in two directions

Since both the coil-array and the two-ring are hollow cylindrical structures transmitter, the rotation of the receiver coil will not have much impact on the system transmission efficiency. This section will explore the offset effect of these two structures in the horizontal direction and vertical direction. Suppose the hori-

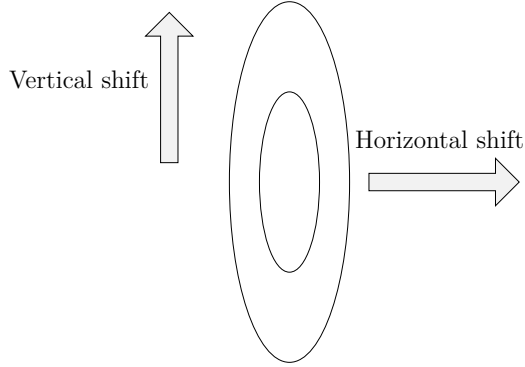


Figure 4.14: Schematic diagram of direction indication.

zontal offset and vertical offset are specified as shown in figure 4.14.

We first offset the internal coils of the two structures from 0 to 100mm in the horizontal direction to obtain the result in figure 4.15 (a). The red line part is the coil-array structure, and the blue part is the two-ring structure. From the figure, we can find that when Rx is in the center of Tx, the transmission efficiency of the two-ring structure is 95%, while the transmission efficiency of the coil-array structure is 60%. And when the horizontal offset increases, the transmission efficiency of the coil-array structure changes greatly, and when the offset is 100mm, the PTE is close to 0. The PTE of the two-ring structure remains basically unchanged.

This is because the coupling of the coil-array structure is completed by small coils. When the horizontal offset exceeds the size of the coil, the opposite circular coil cannot be coupled well, so the PET drops sharply. The coupling of the two-ring structure is the coupling between two hollow cylindrical coils, like two solenoids, so even when a large displacement occurs in the horizontal direction, the PTE can basically remain unchanged.

Figure 4.15 (b) shows the offset in the vertical direction. We can see that the red line representing the coil-array structure increases with the horizontal offset of the Rx coil, that is, the Tx coil and the Rx coil are getting closer, and the PTE of the system is also constantly increase. When the offset reaches 25mm, the PTE of the system is close to 90%.

Although we found that the system transmission efficiency and anti-offset ability of the coil-array structure is not as well as the two-ring structure, but in some

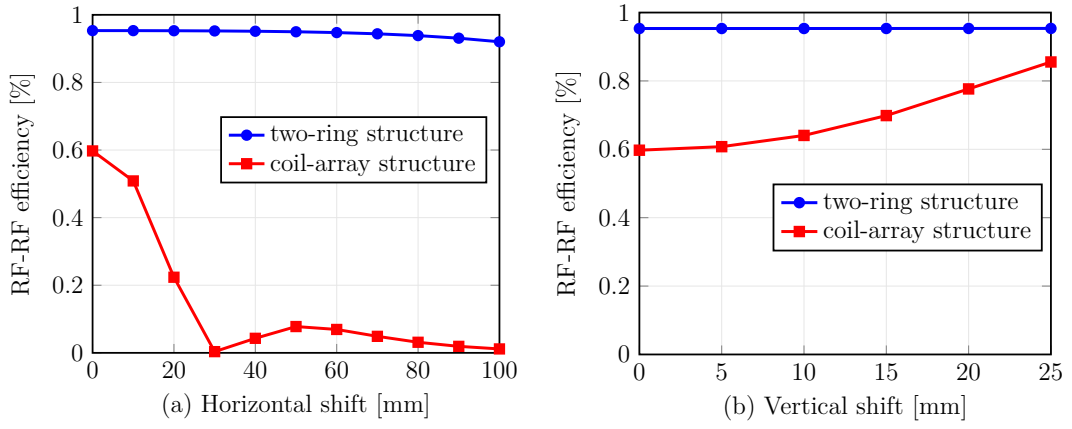


Figure 4.15: The PET over shift in two different directions.

specific occasions (hope that the internal components of the AUV system can get good electromagnetic protection), we prefer to use the coil-array structure for power transmission.

## 5 Conclusion

WPT uses the electric power to electromagnetic field to electric power transmission mode to realize the transmission without electrical contact, and provides a safe and reliable power transmission scheme for underwater sensors and electromechanical equipments. However, under the seawater environment, the electromagnetic coupler has a low coupling coefficient, additional circuit and dielectric loss, and a series of problems such as low transmission efficiency of WPT, which hinder the general application of this technology in the field of marine technology. In this thesis, the electromagnetic radiation, coil offset and transmission efficiency of the non-contact power transmission system in the marine environment are studied on the basis of the preliminary research of the research group. Discussing how to obtain high transmission efficiency and maintain low electromagnetic radiation from multiple perspectives such as system mechanism, simulation calculation, parameter design, coil design, system implementation and experimental testing, has certain academic value and practical significance.

From the perspective of practical application, with full consideration of marine environmental factors, a more detailed and in-depth theoretical study and analysis of the transmission efficiency under different resonance compensation structures and load resistance values are carried out, and the research results are summarized as follows:

Based on the WPT model in the air, an equivalent model of the coils in the seawater environment is proposed. The comparison between the WPT model in the air and the water shows that the seawater medium changes the values of some parameters in the original system, but does not change the wireless energy transmission principle of the system in the air. Therefore, the basic analysis method in seawater environment is: on the basis of analysis of conventional WPT model in the air, combined with the analysis of the comprehensive influence of

seawater media on the parameters of the WPT system, to guide the design of WPT system under seawater.

Through the design and calculation of the resonance compensation structure and its characteristic impedance, the principles and scope of application of two common compensation structures are discussed. And respectively calculate the relationship between their power supply voltage and load voltage and system efficiency. And through two different coil structures to verify these two compensation networks.

The research results have reference and practical value for further in-depth research and system development, perfecting the theory of non-contact transmission technology, and popularizing the application of non-contact transmission technology in the marine field.

## 5.1 Future works

Due to the limitation of time and conditions, the research and work of this article have further in-depth and perfect places:

Because of the difficulty of the simulation and the lack of suitable experimental components, this research has not yet optimized the mini-coils in the coil-array. If we can do more research on the size, type, and shape of these coils, we could get better system performance.

Because it is difficult to analyze the mutual inductance between multiple sets of connected coils in a three-dimensional space, we have not yet analyzed the influence between mini-coils. This makes us wonder how to change the layout of mini-coils to minimize the impact of mini-coils on the UWPT system.

# Acknowledgements

First of all, I would like to thank my supervisor, Professor Minoru Okada. Professor Okada is kind, knowledgeable, and rigorous in scientific attitude. Thank him for giving me an opportunity to study in Japan and let me do wireless power transfer research that I am interested in. He has continued to help me during my three years of study and life. At the same time, I would like to thank Professor Yuichi Hayashi for my research advice and guidance, so that I have a deeper understanding of the weak research environment. With his help, Which greatly improved my research.

Then I would like to thank Associate Professor Takeshi Higashino and Assistant Professor Duong Quang Thang. With their help, they have made me better understand the knowledge of wireless power transfer and wireless communication, and they have helped me overcome the difficulties in professional understanding and helped me complete this topic. Thank them very much. Here, I would also like to thank Assistant Professor Chen Na for her continuous help and encouragement in my studies, so that I have a better understanding of the field of communication.

I would also like to thank the members, staff, and seniors of the Network Systems Laboratory for their companionship in the study and life. We studied together and played together, and established a strong friendship together. Thank you to the international students who have helped me while studying abroad. Thank you for your kindness to me.

Finally, I would like to thank my family for their support of studying abroad, let me choose the knowledge I like, and always provide me with abundant financial support.

Thank you all for your kind help again.

# References

- [1] P. Z. Taofeek Orekan, *Underwater Wireless Power Transfer*. Springer-Verlag GmbH, Dec. 2018. [Online]. Available: [https://www.ebook.de/de/product/35055522/taofeek\\_orekan\\_peng\\_zhang\\_underwater\\_wireless\\_power\\_transfer.html](https://www.ebook.de/de/product/35055522/taofeek_orekan_peng_zhang_underwater_wireless_power_transfer.html)
- [2] J. Randhawa, “Ocean energy: The future of renewable energy,” 07 2015.
- [3] J. Heidemann, M. Stojanovic, and M. Zorzi, “Underwater sensor networks: applications, advances and challenges,” *Philosophical Transactions of the Royal Society A: Mathematical, Physical and Engineering Sciences*, vol. 370, no. 1958, pp. 158–175, jan 2012.
- [4] W. Wu, Z. Zhang, W. Lee, and D.-Z. Du, “Underwater sensors,” in *Optimal Coverage in Wireless Sensor Networks*. Springer International Publishing, 2020, pp. 257–260.
- [5] J. Hwang, N. Bose, and S. Fan, “AUV adaptive sampling methods: A review,” *Applied Sciences*, vol. 9, no. 15, p. 3145, aug 2019.
- [6] N.-H. Tran, T.-D. Huynh, T.-P. Ton, and T.-H. Huynh, “Design of depth control for hybrid AUV,” in *Lecture Notes in Electrical Engineering*. Springer International Publishing, aug 2020, pp. 521–531.
- [7] A. Bradley, M. Feezor, H. Singh, and F. Y. Sorrell, “Power systems for autonomous underwater vehicles,” *IEEE Journal of Oceanic Engineering*, vol. 26, no. 4, pp. 526–538, 2001.
- [8] R. B. Wynn, V. A. Huvenne, T. P. L. Bas, B. J. Murton, D. P. Connelly, B. J. Bett, H. A. Ruhl, K. J. Morris, J. Peakall, D. R. Parsons, E. J. Sumner, S. E. Darby, R. M. Dorrell, and J. E. Hunt, “Autonomous underwater vehicles

- (AUVs): Their past, present and future contributions to the advancement of marine geoscience,” *Marine Geology*, vol. 352, pp. 451–468, jun 2014.
- [9] R. Jurdak, C. Lopes, and P. Baldi, “Battery lifetime estimation and optimization for underwater sensor networks,” *IEEE Sensor Network Operations*, 05 2006.
- [10] B. Taormina, J. Bald, A. Want, G. Thouzeau, M. Lejart, N. Desroy, and A. Carlier, “A review of potential impacts of submarine power cables on the marine environment: Knowledge gaps, recommendations and future directions,” *Renewable and Sustainable Energy Reviews*, vol. 96, pp. 380–391, nov 2018.
- [11] R. Hahn, J. Mainert, F. Glaw, and K.-D. Lang, “Sea water magnesium fuel cell power supply,” *Journal of Power Sources*, vol. 288, pp. 26–35, aug 2015.
- [12] V. E. B. Anand Nayyar, *International Conference on Innovative Computing and Communications*. Springer-Verlag GmbH, Nov. 2018. [Online]. Available: [https://www.ebook.de/de/product/34849820/international\\_conference\\_on\\_innovative\\_computing\\_and\\_communications.html](https://www.ebook.de/de/product/34849820/international_conference_on_innovative_computing_and_communications.html)
- [13] H. Painter and J. Flynn, “Current and future wet-mate connector technology developments for scientific seabed observatory applications,” in *OCEANS 2006*. IEEE, sep 2006.
- [14] T. Wang, D. Li, C. Yang, M. Lin, and T. Zhang, “Non-contact wet mate connectors for subsea observation networks,” in *OCEANS 2016 MTS/IEEE Monterey*. IEEE, sep 2016.
- [15] B. Song, Y. Wang, K. Zhang, and Z. Mao, “Research on wireless power transfer system for torpedo autonomous underwater vehicles,” *Advances in Mechanical Engineering*, vol. 10, no. 9, p. 1687814018802563, 2018. [Online]. Available: <https://doi.org/10.1177/1687814018802563>
- [16] L. Yang, B. Zhang, and M. Ju, “A fast dynamic response regulation method for undersea wireless power transfer system,” in *2019 14th IEEE Conference on Industrial Electronics and Applications (ICIEA)*. IEEE, jun 2019.

- [17] R. Hasaba, K. Okamoto, S. Kawata, K. Eguchi, and Y. Koyanagi, “Magnetic resonance wireless power transfer over 10 m with multiple coils immersed in seawater,” *IEEE Transactions on Microwave Theory and Techniques*, vol. 67, no. 11, pp. 4505–4513, nov 2019.
- [18] T. Orekan, P. Zhang, and C. Shih, “Analysis, design, and maximum power-efficiency tracking for undersea wireless power transfer,” *IEEE Journal of Emerging and Selected Topics in Power Electronics*, vol. 6, no. 2, pp. 843–854, jun 2018.
- [19] S. C. Capareda, “Tidal energy,” in *Introduction to Renewable Energy Conversions*. CRC Press, aug 2019, pp. 239–264.
- [20] B. Drew, A. R. Plummer, and M. N. Sahinkaya, “A review of wave energy converter technology,” *Proceedings of the Institution of Mechanical Engineers, Part A: Journal of Power and Energy*, vol. 223, no. 8, pp. 887–902, dec 2009.
- [21] J. G. Vlachogiannis, “Marine-current power generation model for smart grids,” *Journal of Power Sources*, vol. 249, pp. 172–174, mar 2014.
- [22] Q. Zeng, J. Ma, J. Mo, and Y. Zhang, “Extracting salt difference energy with silicon nitride nanopore generator,” in *2020 5th International Conference on Power and Renewable Energy (ICPRE)*. IEEE, sep 2020.
- [23] Wikipedia contributors, “Wireless power transfer — Wikipedia, the free encyclopedia,” 2021, [Online; accessed 23-January-2021]. [Online]. Available: [https://en.wikipedia.org/w/index.php?title=Wireless\\_power\\_transfer&oldid=1001183613](https://en.wikipedia.org/w/index.php?title=Wireless_power_transfer&oldid=1001183613)
- [24] C. M. Chun T. Rim, *Wireless Power Transfer for Electric Vehicles and Mobile Devices*. IEEE COMPUTER SOC PR, Aug. 2017. [Online]. Available: [https://www.ebook.de/de/product/29045715/chun\\_t\\_rim\\_chris\\_mi\\_wireless\\_power\\_transfer\\_for\\_electric\\_vehicles\\_and\\_mobile\\_devices.html](https://www.ebook.de/de/product/29045715/chun_t_rim_chris_mi_wireless_power_transfer_for_electric_vehicles_and_mobile_devices.html)
- [25] Z. Zhang, H. Pang, A. Georgiadis, and C. Cecati, “Wireless power transfer—an overview,” *IEEE Transactions on Industrial Electronics*, vol. 66, no. 2, pp. 1044–1058, feb 2019.

- [26] A. Shaw, A. Al-Shamma'a, S. Wylie, and D. Toal, "Experimental investigations of electromagnetic wave propagation in seawater," in *2006 European Microwave Conference*. IEEE, sep 2006.
- [27] Y. Wang, B. Song, and Z. Mao, "Application of shielding coils in underwater wireless power transfer systems," *Journal of Marine Science and Engineering*, vol. 7, no. 8, 2019. [Online]. Available: <https://www.mdpi.com/2077-1312/7/8/267>
- [28] C. Jiang, K. T. Chau, C. Liu, and C. H. T. Lee, "An overview of resonant circuits for wireless power transfer," *Energies*, vol. 10, no. 7, p. 894, jun 2017.
- [29] W. Zhang and C. C. Mi, "Compensation topologies of high-power wireless power transfer systems," *IEEE Transactions on Vehicular Technology*, vol. 65, no. 6, pp. 4768–4778, jun 2016.
- [30] Wikipedia contributors, "Relative permittivity — Wikipedia, the free encyclopedia," 2020, [Online; accessed 23-January-2021]. [Online]. Available: [https://en.wikipedia.org/w/index.php?title=Relative\\_permittivity&oldid=991278612](https://en.wikipedia.org/w/index.php?title=Relative_permittivity&oldid=991278612)
- [31] Lenntech, "Water conductivity - lenntech," 2021. [Online]. Available: <https://www.lenntech.com/applications/ultrapure/conductivity/water-conductivity.htm>
- [32] S. Li and C. C. Mi, "Wireless power transfer for electric vehicle applications," *IEEE Journal of Emerging and Selected Topics in Power Electronics*, vol. 3, no. 1, pp. 4–17, mar 2015.
- [33] T. Ohira, "Extended k-q product formulas for capacitive- and inductive-coupling wireless power transfer schemes," *IEICE Electronics Express*, vol. 11, no. 9, pp. 20140147–20140147, 2014.